Identification of biomarkers co-associated with M1 macrophages, ferroptosis and cuproptosis in alcoholic hepatitis by bioinformatics and experimental verification

Shasha Hou[1], Dan Wang[2], Xiaxia Yuan[1], Xiaohuan Yuan[2] and Qi Yuan[2]*

[1]Department of Life Science and Engineering, Jining University, Jining, China, [2]College of Life Science, Mudanjiang Medical University, Mudanjiang, China

Backgrounds: Alcoholic hepatitis (AH) is a major health problem worldwide. There is increasing evidence that immune cells, iron metabolism and copper metabolism play important roles in the development of AH. We aimed to explore biomarkers that are co-associated with M1 macrophages, ferroptosis and cuproptosis in AH patients.

Methods: GSE28619 and GSE103580 datasets were integrated, CIBERSORT algorithm was used to analyze the infiltration of 22 types of immune cells and GSVA algorithm was used to calculate ferroptosis and cuproptosis scores. Using the "WGCNA" R package, we established a gene co-expression network and analyzed the correlation between M1 macrophages, ferroptosis and cuproptosis scores and module characteristic genes. Subsequently, candidate genes were screened by WGCNA and differential expression gene analysis. The LASSO-SVM analysis was used to identify biomarkers co-associated with M1 macrophages, ferroptosis and cuproptosis. Finally, we validated these potential biomarkers using GEO datasets (GSE155907, GSE142530 and GSE97234) and a mouse model of AH.

Results: The infiltration level of M1 macrophages was significantly increased in AH patients. Ferroptosis and cuproptosis scores were also increased in AH patients. In addition, M1 macrophages, ferroptosis and cuproptosis were positively correlated with each other. Combining bioinformatics analysis with a mouse model of AH, we found that ALDOA, COL3A1, LUM, THBS2 and TIMP1 may be potential biomarkers co-associated with M1 macrophages, ferroptosis and cuproptosis in AH patients.

Conclusion: We identified 5 potential biomarkers that are promising new targets for the treatment and diagnosis of AH patients.

KEYWORDS

alcoholic hepatitis, M1 macrophage, ferroptosis, cuproptosis, WGCNA

Introduction

Alcohol-associated liver disease (ALD) is a serious public health problem worldwide (1). Alcoholic hepatitis (AH) is one of the phenotypes of ALD, which is mainly caused by a long history of excessive alcohol consumption and a recent history of severe alcohol abuse (2). AH presents a clinical syndrome characterized by jaundice and liver injury. In the past 50 years, corticosteroids are still the main therapeutic drugs, and no effective new drugs have been successfully developed (3). Although corticosteroids increase short-term survival in AH patients, approximately 40% of patients do not respond to treatment (4, 5). In recent years, the rapid development of high-throughput sequencing technology has promoted the understanding of AH (6, 7). Therefore, it is urgently needed to identify new biomarkers in AH patients by bioinformatics analysis, which will facilitate the development of new treatment strategies.

The liver plays a major regulatory role in alcohol metabolism and immune monitoring. Hepatocytes exposed to alcohol cause damage and death due to oxidative stress, which in turn produces a variety of inflammatory factors to activate the inflammatory response and immune cells (8). Macrophages are important cells of innate immune system. The complex functional variability and adaptability of macrophages to different infection situations are based on their extensive phenotypic plasticity. naive macrophages (M0) can be polarized into classically activated macrophages (M1 macrophages) and alternately activated macrophages (M2 macrophages), which perform proinflammatory or anti-inflammatory functions, respectively (9). Previous studies have shown that damaged hepatocytes activate the NF-κB signaling pathway under alcohol metabolism, which releases a series of chemokines and inflammatory mediators, ultimately promoting macrophage M1 polarization (10, 11). In addition, Cho et al. revealed that G-CSF improved liver function by promoting macrophage M2 polarization in alcohol-fed mice (12).

Ferroptosis is a unique type of cell death regulation, which is caused by iron accumulation, excessive production of reactive oxygen species (ROS) and excessive lipid peroxidation (13). Cuproptosis is a recently discovered type of cell death caused by the direct binding of copper to the lipidized proteins of the mitochondrial tricarboxylic acid cycle (TCA) (14). Alcohol metabolism in hepatocytes affects mitochondrial function and produces a large number of ROS, leading to elevated lipid peroxidation. Thus, the progression of AH is closely related to ferroptosis and cuproptosis. As recently reported, intestinal sirtuin1 (SIRT1) deficiency protects mice from alcohol-induced inflammation by mitigating hepatic ferroptosis (15). Melatonin inhibits ferroptosis by activating Nrf2-ARE signaling pathway, thus alleviating alcohol-induced liver injury (16). Copper metabolism in the liver is still being explored. Cuproptosis regulates immune cell infiltration and is used to construct risk assessment models for hepatocellular carcinoma (HCC) (17, 18). However, the role of ferroptosis and cuproptosis in AH patients needs to be further explored.

In this study, we downloaded and integrated transcriptome data from AH patients. Potential biomarkers of AH patients were

identified based on the M1 macrophages, ferroptosis and cuproptosis scores, and these biomarkers were validated using public datasets and a mouse model of AH. Finally, we identified 5 potential biomarkers: aldolase A (ALDOA), Collagen type III alpha 1 (COL3A1), lumican (LUM), thrombospondin-2 (THBS2) and tissue inhibitor of metalloproteinase-1 (TIMP1). These potential biomarkers could provide new targets for the diagnosis and treatment of AH patients.

Materials and methods

Data set download and evaluation

Gene expression data were downloaded from the Gene Expression Integrated Database (GEO)(http://www.ncbi.nlm.nih.gov/geo/) with accession numbers GSE28619 (19), GSE103580 (20), GSE155907 (21), GSE142530 (7) and GSE97234 (22), the basic information of our selected samples is shown in Supplementary Table S1. The batch effect between GSE28619 and GSE103580 was corrected using the "sva" R package (23). The intersected genes between GSE28619 and GSE103580 were obtained *via* online Venn Diagram analysis (jvenn, http://jvenn.toulouse.inra.fr/app/index.html).

Analysis of immune cells

The CIBERSORT algorithm was used to calculate the proportion of 22 types of immune cells with normalized gene expression data (24). Correlations between immune cells were evaluated using the "corrplot" R package. Based on the characteristics of immune cells, principal component analysis (PCA) was to cluster the normal liver samples and AH samples. Specifically, the "stats" R package was used for PCA analysis. Firstly, z-score was performed on the expression profile, and then prcomp function was used for dimension reduction analysis to obtain the matrix after dimension reduction.

Gene set variation analysis

The "GSVA" R package (25) was used to calculate the scores of ferroptosis gene set and cuproptosis gene set. A total of 64 ferroptosis-related genes were obtained from MigDB (Supplementary Table S2). The 16 cuproptosis-related genes were collected from previous literature (26) (Supplementary Table S3).

Weighted gene co-expression network analysis

WGCNA is an algorithm for constructing gene clustering modules based on similar gene expression patterns. We used the "WGCNA" R package (27) to construct a co-expression network of genes from normal liver samples and AH samples. The concrete

steps are as follows: First, the optimal soft-thresholding power was calculated and selected. Second, the adjacency matrix was constructed based on the selected soft-thresholding power and transformed into a topological overlap matrix. Third, hierarchical clustering tree was established to cluster high-coexpression genes into the same module. Finally, M1 macrophages, ferroptosis and cuproptosis scores were used as characteristics to calculate the correlation between module genes and traits. In this study, we screened hub genes based on threshold weight > 0.2, and Cytoscape software (version 3.9.1) was used to visualize the gene networks.

Functional enrichment analysis

To further clarify biological functions and signaling pathways of candidate genes, we used the "clusterProfiler" R package (28) for functional enrichment analysis, including gene ontology (GO) and Kyoto Encyclopedia of Genes and Genomes (KEGG) analysis. The result of functional enrichment analysis was visualized using the "GOplot" R package (29).

Analysis of differentially expressed genes

We used the "limma" R package (30) to calculate differentially expressed genes (DEGs) between normal liver samples and AH samples. DEGs were obtained by threshold standard $|log2(FC)| > 1$, p-value < 0.05. The volcano and heatmap plots were visualized *via* the "ggplot2" and "pheatmap" R packages.

Machine learning

By intersecting DEGs and WGCNA hub genes, 27 candidate genes associated with AH patients were identified. For these 27 candidate genes, two machine-learning techniques were used to further screen potential genes in AH patients. The least absolute shrinkage and selection operator (LASSO) is an algorithm used for regularization to improve prediction accuracy and model comprehensibility, and to select variables. We utilized the LASSO algorithm to screen potential biomarkers in AH patients by "glmnet" R package (31). Support vector machines (SVM) is a powerful method whose goal is to establish a threshold between two classes that allows label prediction based on single or multiple feature vectors. We used SVM method to screen potential biomarkers in AH patients by "kernlab" R package (32). The intersection of the results between the two methods were obtained *via* online Venn Diagram analysis (jvenn, http://jvenn.toulouse.inra.fr/app/index.html). To further assess the ability of biomarkers to distinguish AH samples from normal liver samples, we performed receiver operating characteristic (ROC) analysis using the "pROC" R package (33).

A mouse model of AH

As previously mentioned, a mouse model of chronic alcohol plus single binge drinking was established (34). The alcoholic diet was purchased from TROPHIC (Nantong, China). Ten male mice aged 6-8 weeks were fed a liquid control diet for 5 days, then mice were randomly divided into two groups (ethanol-fed group and pair-fed group, n = 5 per group). The ethanol-fed group was fed a Lieber DeCarli liquid diet containing 5% ethanol for 10 days. Then mice were given a single dose of 20% ethanol (5g/kg body weight) by gavage. The pair-fed group was fed with ethanol-free, isocaloric control liquid diet for 10 days. Then mice were given a single dose of dextrin maltose (5g/kg body weight) by gavage. Euthanasia was performed 9 hours after gavage. All animal experiments were performed with the approval of the Experimental Animal Ethics Committee of Mudanjiang Medical University.

Blood biochemical assays

Blood samples of mice were centrifuged at 1000×g for 10 min to obtain serum. Serum alanine aminotransferase (ALT) and aspartate aminotransferase (AST) levels were detected by kits of Nanjing Jiancheng Bioengineering Institute (Nanjing, China).

Content analysis of malondialdehyde (MDA) and glutathione

Liver tissues were homogenized according to the instructions, and MDA and GSH levels were detected by kits of Nanjing Jiancheng Bioengineering Institute (Nanjing, China).

Histology and immunofluorescence

Paraffin or cryostat sections were prepared as described previously (35). Paraffin sections were stained with hematoxylin and eosin (H&E). For fluorescence double staining, cryostat sections were incubated with anti-iNOS antibody (Santa Cruz Biotechnology, Santa Cruz, CA, USA) and anti-F4/80 antibodies (BioLegend, San Diego, CA, USA), followed by incubation with Alexa Fluor 488- or 594-conjugated secondary antibodies (Jackson ImmunoResearch, West Grove, PA, USA). Sections were evaluated under a microscope (DP71, OLYMPUS) of both bright-field and fluorescence microscopy (200 × magnification).

Real-time quantitative PCR

Total RNA was isolated from liver tissues using TRIzol reagent (TransGen Biotech, Beijing, China), and cDNAs were synthesized

using FastKing RT Kit (TIANGEN, Beijing, China). RT-qPCR analysis was performed using SuperReal PreMix Plus (TIANGEN, Beijing, China). The primer sequences were listed in Supplementary Table S4. Data were analyzed using the $2^{-\Delta\Delta CT}$ method and normalized to β-actin (*Actb*) expression.

Western blot

Total protein from liver tissue was extracted using RIPA lysis buffer (Solarbio, Beijing, China) containing protease inhibitor cocktail (MedChemExpress, Princeton, NJ, USA). The samples were incubated at 99°C for 5 min and separated at 115 V by SDS-PAGE for 1 h. The proteins were transferred to PVDF membranes and incubated at 200 mA for 1 h. The membrane was plugged with 5% milk powder for 1 hour and incubated overnight at 4°C with the following primary antibody: anti-FDX1 (Absin, Shanghai, China), anti-GPX4, anti-ACSL4, anti-SLC31A1 and anti-β-actin (Affinity, Cincinnati, OH, USA). HRP-conjugated goat anti-rabbit IgG was used as secondary antibodies. All bands were quantified with an automated digitizing system (ImageJ).

Statistical analysis

All data were presented as mean ± SD and analyzed using GraphPad Prism (version 8.3.0) and R (version 4.2.1). Significant differences in animal experiments were determined by three independent experiments. Differences of continuous variables between two groups were compared using Student's t-test analysis. $P < 0.05$ was considered statistically significant.

Results

Overview of study design

The overall design scheme of our current study is shown in Figure 1. First, we combined and normalized data of GSE28619 and GSE103580. Secondly, CIBERSORT method was used to analyze immune cells, GSVA algorithm was used to calculate scores of ferroptosis and cuproptosis, and WGCNA was used to screen hub genes related to M1 macrophages, ferroptosis and cuproptosis. Third, we analyzed DEGs using the "limma" package and intersected DEGs with hub genes. Fourth, we identified biomarkers of AH based on LASSO-SVM algorithm. Finally, we used GEO data (GSE155907, GSE142530 and GSE97234) and a mouse model of AH to validate potential biomarkers.

Normalization of dataset

Both GSE28619 and GSE103580 datasets are chip data. The GSE28619 dataset was based on the GPL570 platform (Affymetrix Human Genome U133 Plus 2.0 Array) and included 7 normal liver samples and 15 AH samples. The GSE103580 dataset was based on the GPL13667 platform (Affymetrix Human Genome U219 Array) from which 13 AH samples were selected. The two datasets were merged and batch removed. The results before and after normalization are shown in Supplementary Figure S1A. As shown in the Venn Diagram (Supplementary Figure S1B), 22,878 and 19,469 probes were identified in GSE28619 and GSE103580, respectively, and 16,510 intersected genes were selected from two datasets for subsequent bioinformatics analysis.

FIGURE 1
Overall schematic diagram of the study design. *p < 0.05, **p < 0.01, ***p < 0.001, ****p < 0.0001.
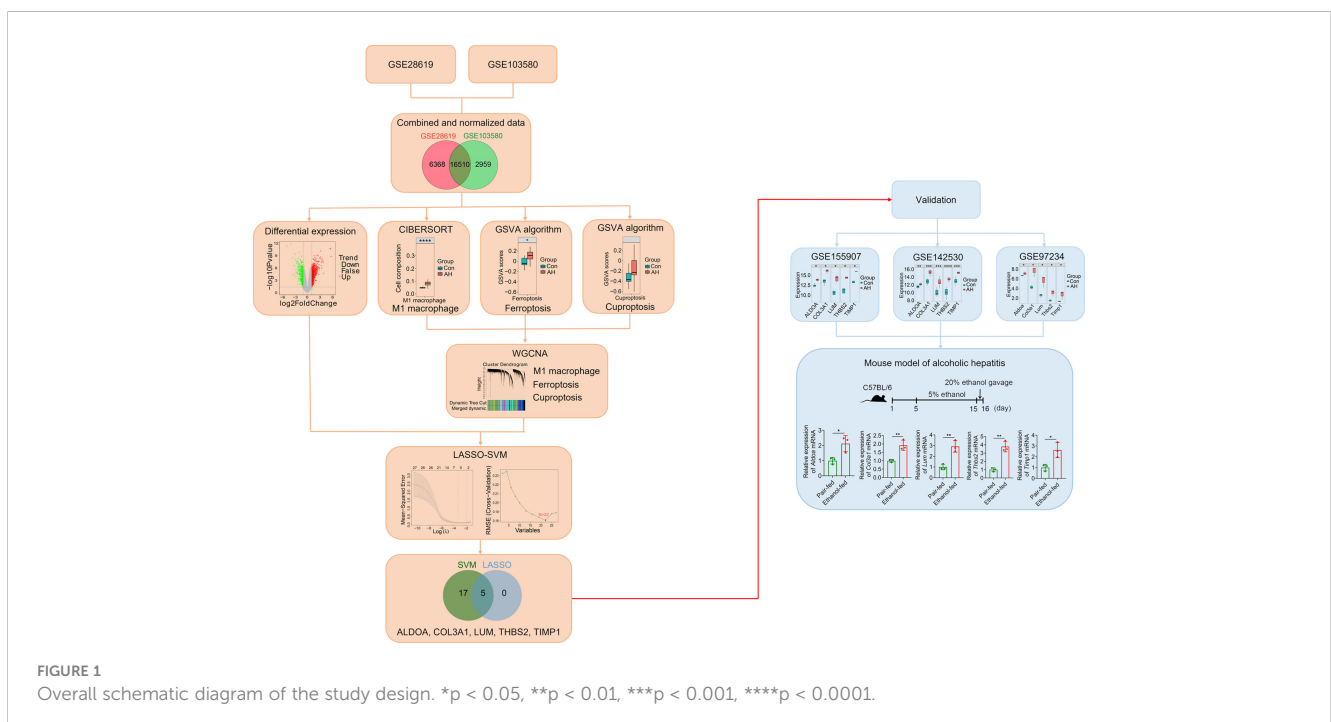
Analysis of immune infiltration in normal liver and AH samples

CIBERSORT, the deconvolution algorithm reported by Newman et al., characterizes cell composition in complex tissues based on 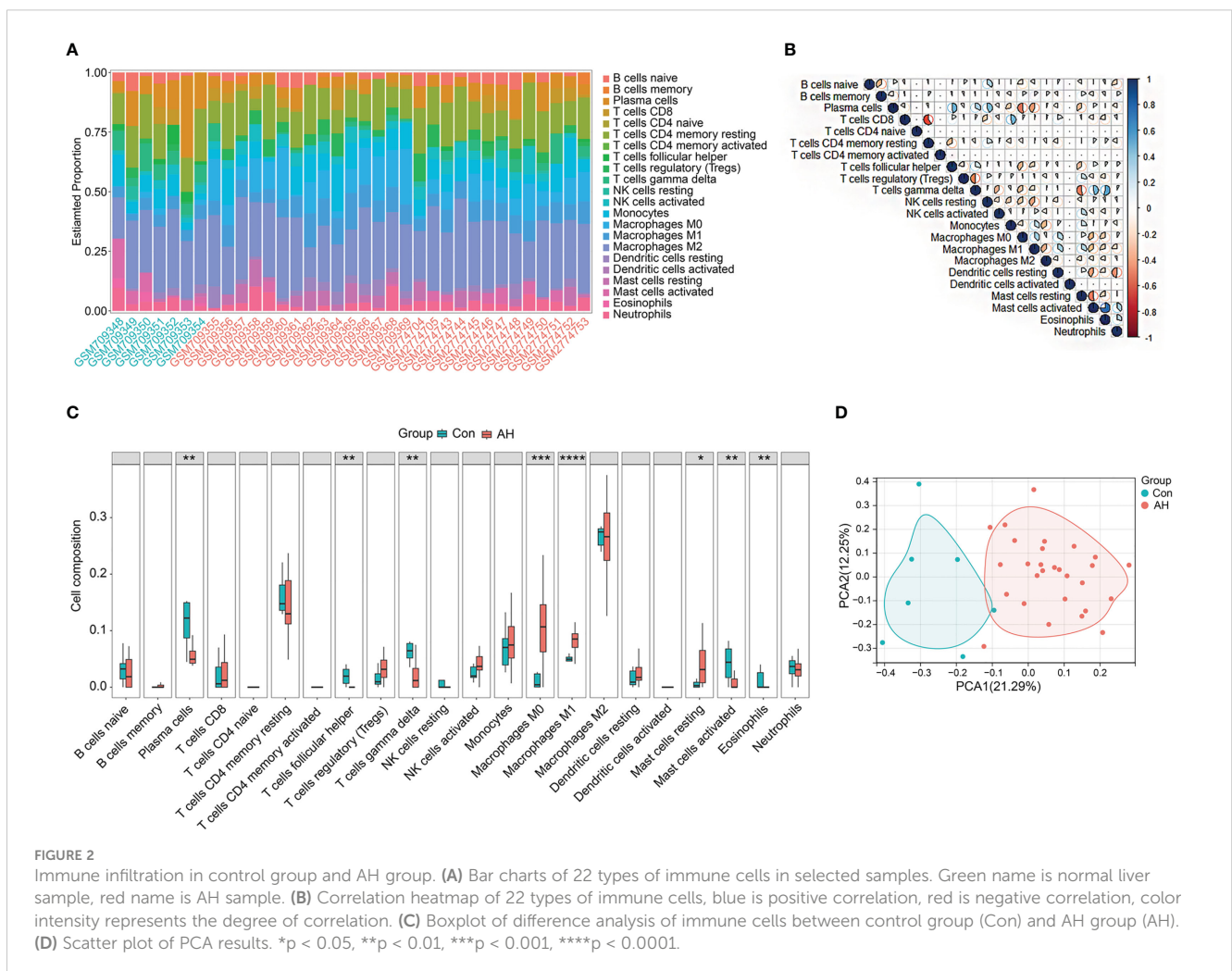normalized gene expression profiles (24). Based on this algorithm, we calculated the infiltration of 22 types of immune cells in normal liver samples and AH samples. The bar chart shows the abundance of different immune cell subsets in each sample (Figure 2A). We further analyzed the correlation between 22 immune cell subsets. As shown in the correlation heatmap (Figure 2B), activated mast cells showed the most significant positive correlation with eosinophils (r = 0.75), while CD8 T cells showed the most significant negative correlation with CD4 memory resting T cells (r = -0.61). Next, we analyzed the difference in immune cells between normal liver samples (control group) and AH samples (AH group). Compared with control group, M0 macrophages, M1 macrophages and resting mast cells were significantly increased in AH group, while plasma cells, helper follicular T cells, gamma delta T cells, activated mast cells and eosinophils were significantly decreased in AH group (Figure 2C). PCA analysis of control group and AH group and performed based on 22 types of immune cells. As shown in Figure 2D, AH group was

completely separated from control group, suggesting that activation of immune cells could be a significant feature of AH patients.

Co-expression modules of M1 macrophages, ferroptosis and cuproptosis in AH patients

We found that M1 macrophages were the most differentiated immune cells between control and AH groups (Figure 2C). At the same time, the GSVA algorithm was used to calculate scores of ferroptosis and cuproptosis. Compared with the control group, ferroptosis scores of the AH group were significantly increased. Although there was no statistical difference in GSVA scores of cuproptosis, there was a increasing trend (Figure 3A). In addition, correlation analysis showed that M1 macrophages, ferroptosis and cuproptosis were positively correlated with each other (Figure 3B). To further explore the role of genes co-associated with M1 macrophages, ferroptosis and cuproptosis in AH patients, we used CIBERSORT's M1 macrophage results, ferroptosis and cuproptosis scores as characteristic data for WGCNA analysis. The power value is set as β value when the correlation coefficient between connectivity K and logarithm logarithm (P(k)) reaches

FIGURE 2

Immune infiltration in control group and AH group. **(A)** Bar charts of 22 types of immune cells in selected samples. Green name is normal liver sample, red name is AH sample. **(B)** Correlation heatmap of 22 types of immune cells, blue is positive correlation, red is negative correlation, color intensity represents the degree of correlation. **(C)** Boxplot of difference analysis of immune cells between control group (Con) and AH group (AH). **(D)** Scatter plot of PCA results. *p < 0.05, **p < 0.01, ***p < 0.001, ****p < 0.0001.
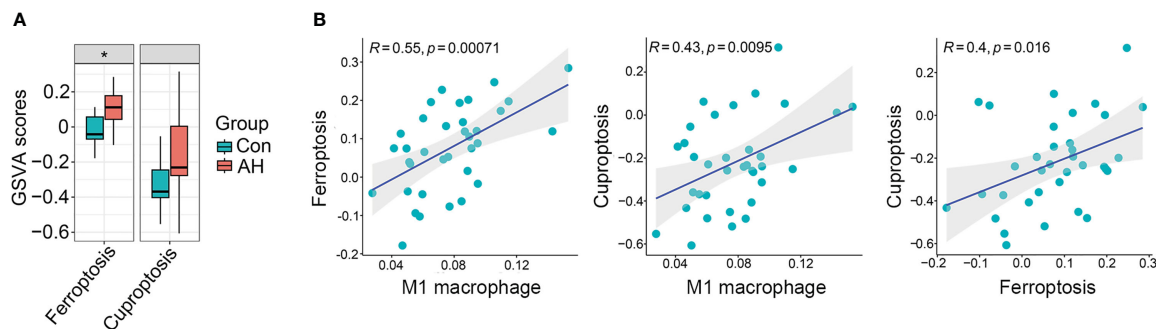
FIGURE 3
M1 macrophages, ferroptosis and cuproptosis were positively correlated with each other. **(A)** Boxplot of difference analysis of ferroptosis and cuproptosis GSVA scores between control group (Con) and AH group (AH). **(B)** Correlation analysis of M1 macrophage, ferroptosis and cuproptosis. *p < 0.05.

0.83. A scale-free topological network (β = 6) was established (Figure 4A). Based on selected soft-thresholding power, a hierarchical clustering tree was established to cluster high-coexpression genes into same module and color code them (Figure 4B). Next, Spearman correlation analysis was used to draw module-trait relationship heatmap for 13 transcription modules identified and evaluate relationship between modules (Figure 4C). We found that red module was closely correlated with M1 macrophages, ferroptosis and cuproptosis, and was also highly correlated with AH traits. Therefore, this module was identified as hub module (Figures 4C, D). The module contains 834 genes, including 33 genes and 41 edges with threshold weight > 0.2 (Figure 4E). These genes are considered as hub genes.

Candidate genes co-associated with M1 macrophages, ferroptosis and cuproptosis in AH patients

To further identify biomarkers associated with AH patients, DEGs analysis was performed on gene expression data from control and AH groups. There were a total of 877 DEGs, including 519 up-regulated genes and 358 down-regulated genes (Figure 5A) (Supplementary Table S5). The intersection of DEGs with hub genes related to M1 macrophages, ferroptosis and cuproptosis was performed to obtain 27 candidate genes (Figure 5B). The heatmap shows expression of these candidate genes in each sample (Figure 5C). Functional enrichment analysis was conducted for the above 27 candidate genes. The top 10 significantly enriched GO terms and KEGG pathways are shown separately in Figures 5D, E (see Supplementary Table S6 for details). AGE-RAGE and PI3K-AKT signaling pathway are associated with inflammation and oxidative stress. This suggests that M1 macrophages, ferroptosis and cuproptosis may be related to each other through the above signaling pathways. In addition, the results of functional enrichment analysis showed that the common high expression of M1 macrophages, ferroptosis and cuproptosis may activate extracellular matrix (ECM)-related signaling pathways.
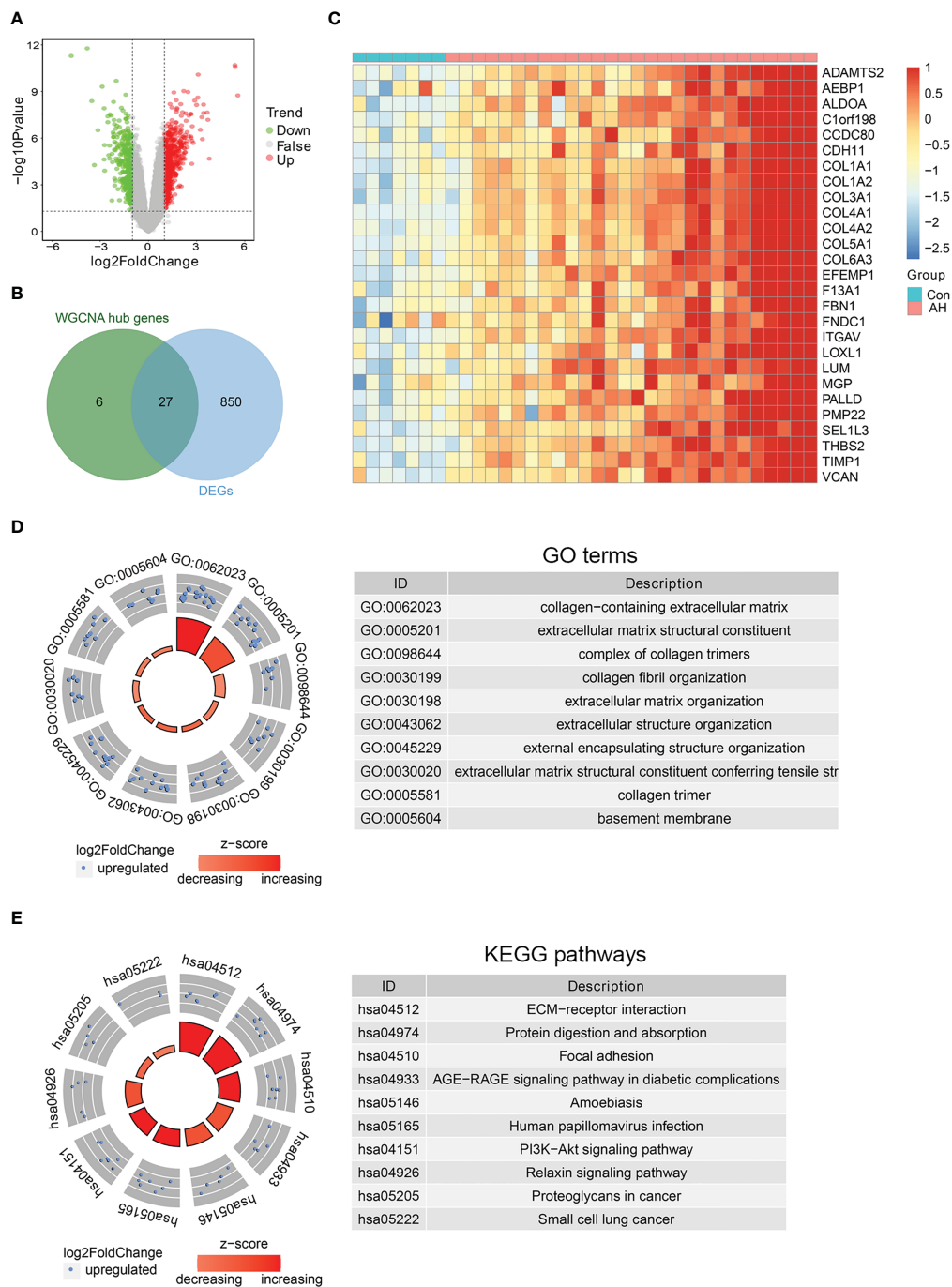
Identification of biomarkers co-associated with M1 macrophages, ferroptosis and cuproptosis *via* machine learning

For the above 27 candidate genes, SVM and LASSO regression algorithms were used to screen potential biomarkers co-associated with M1 macrophages, ferroptosis and cuproptosis. According to the results of ten fold cross-validation in SVM algorithm, 22 feature genes were identified (Figure 6A, Table 1). The coefficients of LASSO versus log (λ) are shown in Figure 6B that 5 feature genes were obtained (Table 1 and Supplementary Table S7). Finally, 5 genes selected by two machine learning algorithms were overlapped, including ALDOA, COL3A1, LUM, THBS2 and TIMP1 (Figure 6C). To assess predictive accuracy of these biomarkers, ROC curves of 5 genes were analyzed (Figure 6D). The AUC values indicated that 5 biomarkers co-associated with M1 macrophages, ferroptosis and cuproptosis had excellent diagnostic values. Next, we analyzed the correlation between 5 potential biomarkers and M1 macrophage, ferroptosis and cuproptosis. The analysis results showed that 5 potential biomarkers were positively correlated with M1 macrophage, ferroptosis and cuproptosis (Figures 7A–C), and 5 potential biomarkers were also positively correlated with each other (Supplementary Figure S2). In addition, we validated 5 potential biomarkers using GSE155907 and GSE142530 datasets. In two validation datasets, consistent with training dataset, all 5 genes in AH group were up-regulated, with statistical significance (Figures 7D, E). Combined with the above results, 5 genes co-associated with M1 macrophages, ferroptosis and cuproptosis can be used as potential biomarkers in AH patients.

Potential biomarkers were validated in a mouse model of AH

To verify 5 potential biomarkers, we first analyzed mouse dataset (GSE97234) and found that the expression levels of 5 genes were significantly up-regulated in AH group (Figure 8A). Based on the above analysis, we conducted experimental

FIGURE 4
Hub gene screening based on WGCNA. **(A)** Scale-free fitting index analysis of soft-thresholding powers. **(B)** Cluster dendrogram. **(C)** Module-trait correlation heatmap, red is positive correlation, blue is negative correlation. **(D)** Scatter plot of red module. Horizontal axis (MM) represented the correlation between genes and modules, and vertical axis (GS) represented the absolute value of correlation between genes and phenotypic characteristics. **(E)** The network of hub genes.

verification in mice. We established a chronic plus single binge alcohol model, which has been widely used to study the pathogenesis of AH (Figure 8B). Compared with pair-fed mice, ethanol-fed mice had a significant decrease in body weight (Figure 8C) and a significant increase in liver weight/body weight ratio (mean, 0.056 vs. 0.048, $P = 0.028$) (Figure 8D). ALT and AST, important indicators of liver injury, were significantly elevated in ethanol-fed mice than in pair-fed mice (ALT, mean, 112.7 vs. 69.1, $P = 0.001$) (AST, mean, 464.0 vs. 269.7, $P = 0.0003$) (Figures 8E, F). H&E staining showed that ethanol feeding resulted in necrosis of hepatocytes and morphological changes of liver tissues, suggesting more severe liver injury in ethanol-fed mice than in pair-fed mice (Figure 8G).

Macrophages play a crucial role in regulating liver homeostasis and hepatic injury. By double immunofluorescence staining of liver

tissues with F4/80 (a marker of macrophage) and iNOS (a marker of M1 macrophage), we found that M1 macrophages (F4/80 and iNOS double positive cells) were almost not expressed in pair-fed mice, while the expression of M1 macrophage marker protein was increased in ethanol-fed mice, suggesting the infiltration of more M1 macrophages (Figure 8H). Lipid peroxide and GSH are crucial markers of ferroptosis. MDA is considered to be the end product of the lipid peroxidation process. The MDA and GSH levels of liver tissues were detected by kits. Compared with pair-fed mice, MDA levels (mean, 2.26 vs. 1.17, $P = 0.021$) were significantly increased and GSH levels (mean, 2.24 vs. 5.41, $P = 0.014$) were significantly decreased in ethanol-fed mice (Figures 9A, B). In addition, the well-identified markers of ferroptosis, GPX4 and ACSL4, were detected in liver tissues by western blot. As shown in Figure 9C, the protein expression levels of GPX4 (mean, 0.40 vs. 0.85, $P = 0.048$) were
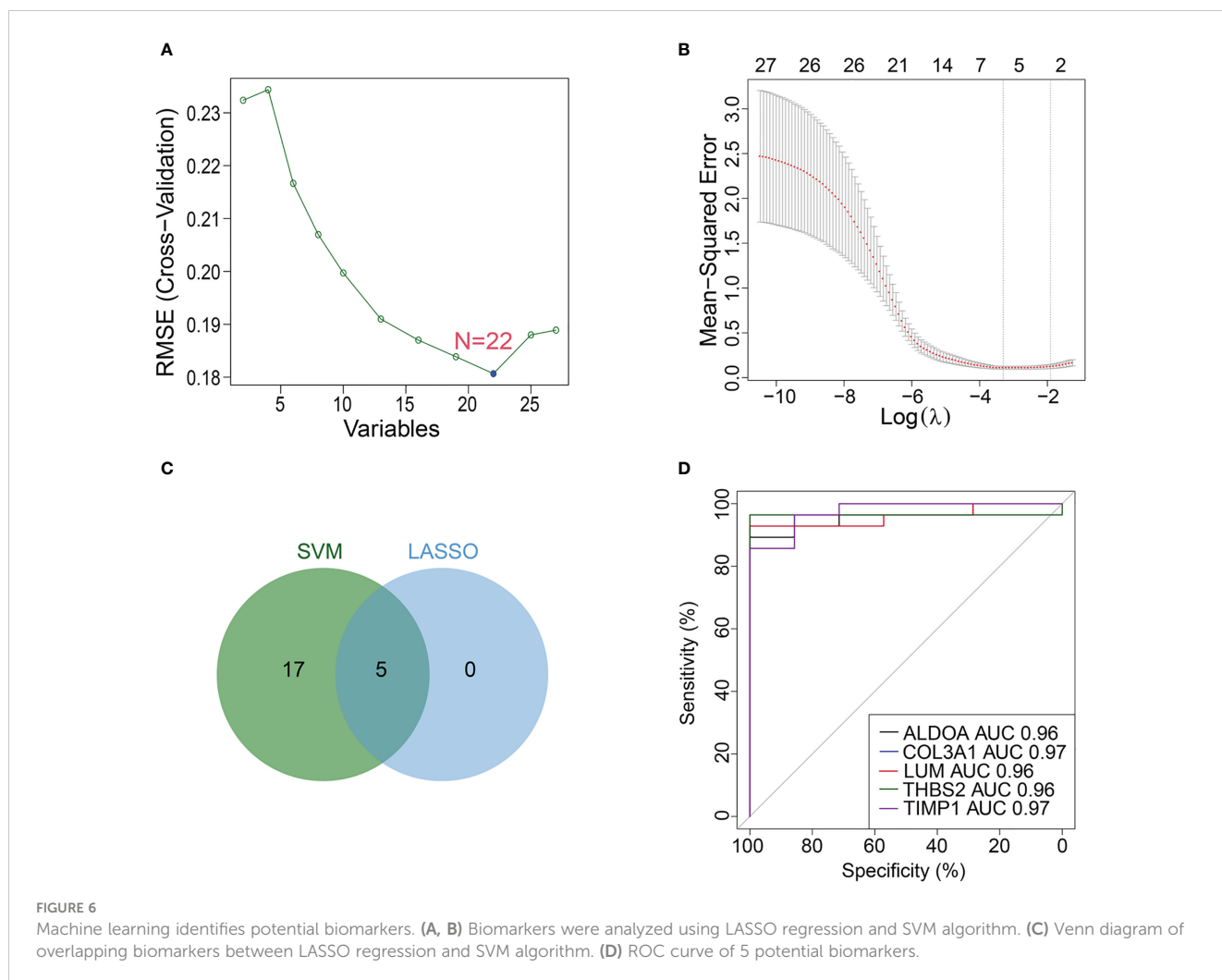
FIGURE 5
Identification of biomarkers co-associated with M1 macrophages, ferroptosis and cuproptosis. **(A)** Volcano plot of DEGs between control and AH groups. **(B)** Venn diagram of intersection genes between DEGs and hub genes. **(C)** The heatmap of 27 candidate genes. **(D)** GO enrichment analysis. **(E)** KEGG enrichment analysis.

significantly down-regulated and the protein expression levels of ACSL4 (mean, 2.29 vs. 0.50, *P* = 0.004) were significantly up-regulated in ethanol-fed mice compared with pair-fed mice. Known biomarkers of cuproptosis, including FDX1 and SLC31A1 were determined. We also detected the expression levels of FDX1 and SLC31A1 in liver tissues by western blot. the protein expression levels of FDX1 (mean, 0.45 vs. 1.25, *P* = 0.031) were significantly down-regulated and the protein expression levels of SLC31A1

(mean, 2.68 vs. 0.75, *P* = 0.022) were significantly up-regulated in ethanol-fed mice compared with pair-fed mice (Figure 9D). Combined with the above results, alcohol consumption significantly promoted the infiltration of M1 macrophages, the expression of ferroptosis and cuproptosis.

The expression levels of *Aldoa*, *Col3a1*, *Lum*, *Thbs2* and *Timp1* mRNA were detected by RT-qPCR. As shown in Figure 9E, compared with pair-fed mice, the expression levels of *Aldoa*

FIGURE 6
Machine learning identifies potential biomarkers. **(A, B)** Biomarkers were analyzed using LASSO regression and SVM algorithm. **(C)** Venn diagram of overlapping biomarkers between LASSO regression and SVM algorithm. **(D)** ROC curve of 5 potential biomarkers.

(mean, 2.12 vs. 1.00, P = 0.027), *Col3a1* (mean, 1.92 vs. 1.00, P = 0.007), *Lum* (mean, 2.92 vs. 1.00, P = 0.005), *Thbs2* (mean, 3.79 vs. 1.00, P = 0.002) and *Timp1* (mean, 2.62 vs. 1.00, P = 0.021) in liver tissues of ethanol-fed mice were significantly increased. These experimental results further support that 5 genes as potential biomarkers for AH patients.
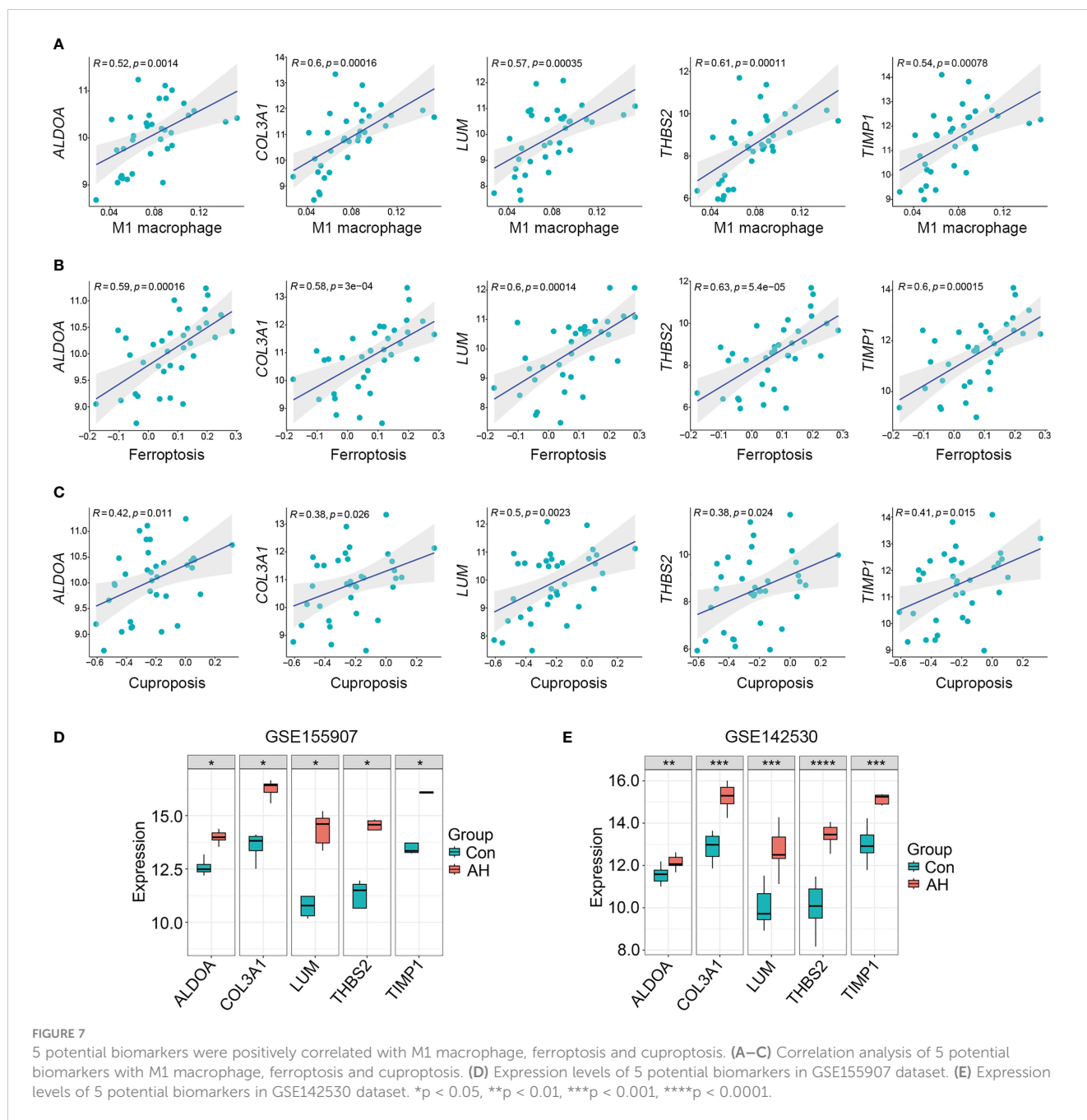
Discussion

In this study, biomarkers co-associated with M1 macrophages, ferroptosis and cuproptosis were identified in AH patients. The CIBERSORT algorithm was used to calculate infiltration of 22 types of immune cells. Ferroptosis and cuproptosis scores were calculated using GSVA algorithm. By WGCNA and LASSO-SVM analysis, we found that ALDOA, COL3A1, LUM, THBS2 and TIMP1 were potential biomarkers in AH patients. These biomarkers were validated in GEO datasets and a mouse model of AH.

Excessive alcohol consumption directly damages hepatocytes, which in turn induces immune cell infiltration and secretion of inflammatory factors, ultimately leading to overactivation of inflammatory cascade (36, 37). For example, neutrophil infiltration and high expression of pro-inflammatory factors (TNF-α and IL-1β) promote the progression of alcohol-related inflammatory response (38). In addition, chronic alcohol consumption leads to upregulation of M1 macrophage-related markers (39). In this study, we used the CIBERSORT algorithm to assess the difference in immune cells between normal liver and AH samples. We found that M1 macrophages were significantly increased in AH patients. These findings provide new insights into immune cell infiltration in AH patients based on transcriptomic analysis.

Clinical calculators such as the Model of End-stage Liver Disease (MELD) score can predict patient mortality and guide clinical treatment strategies (40). However, MELD score is not specifically designed to predict AH. Clinically, biomarkers for AH prediction have not been identified. Therefore, the discovery of new biomarkers for AH prediction is an urgent area of research. In recent years, with the development of high-throughput sequencing technology, the identification of disease-related biomarkers based

FIGURE 7

5 potential biomarkers were positively correlated with M1 macrophage, ferroptosis and cuproptosis. **(A–C)** Correlation analysis of 5 potential biomarkers with M1 macrophage, ferroptosis and cuproptosis. **(D)** Expression levels of 5 potential biomarkers in GSE155907 dataset. **(E)** Expression levels of 5 potential biomarkers in GSE142530 dataset. *p < 0.05, **p < 0.01, ***p < 0.001, ****p < 0.0001.

on transcriptomic analysis has been widely studied. In previous studies, a prognostic model of hepatocellular carcinoma was established using WGCNA analysis of macrophage-related genes (41). The prognostic model based on ferroptosis and epithelial-mesenchymal transition state helps predict overall survival of hepatocellular carcinoma (42). Cuproptosis-related subtypes predict tumor microenvironments and drug candidates in hepatocellular carcinoma (43). However, biomarkers for AH

TABLE 1 Feature genes obtained by machine learning.

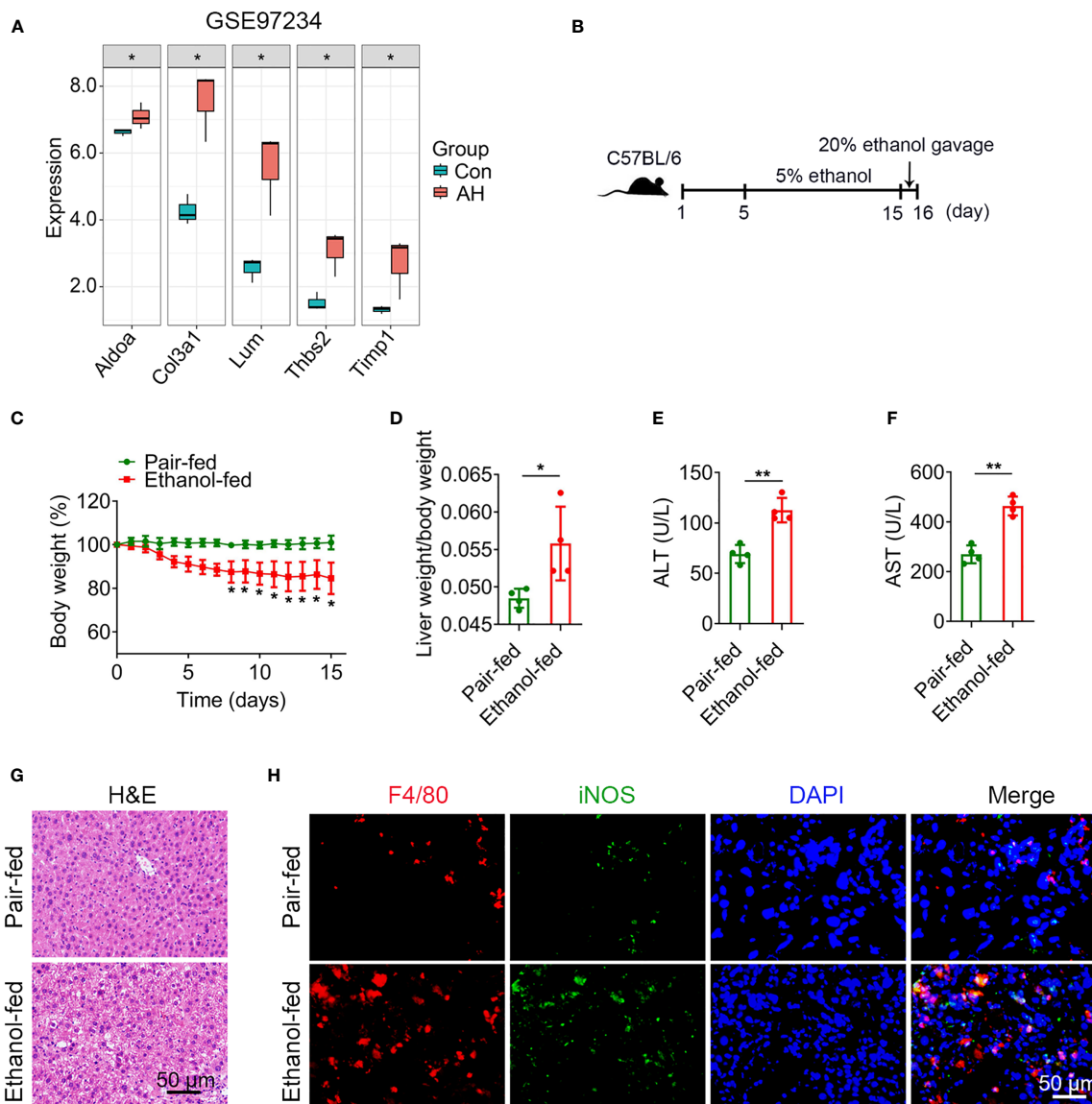| Machine learning	Feature genes
SVM	CCDC80, COL5A1, ITGAV, CDH11, VCAN, THBS2, COL4A2, COL4A1, SEL1L3, PMP22, C1orf198, FBN1, PALLD, COL1A2, COL3A1, EFEMP1, TIMP1, ALDOA, LUM, ADAMTS2, COL6A3, COL1A1
LASSO	ALDOA, COL3A1, LUM, THBS2, TIMP1

FIGURE 8

Alcohol exposure promotes infiltration of M1 macrophages. **(A)** Expression levels of 5 potential biomarkers in GSE97234 dataset. **(B–H)** Groups of C57BL/6 mice (n = 5 per group) were fed ethanol liquid diet or ethanol free control liquid diet. **(B)** Schematic diagram of a chronic binge eating model. **(C)** Changes in body weight. **(D)** Liver weight/body weight change ratio. **(E, F)** Serum ALT and AST levels. **(G)** Representative H&E staining of liver tissues. Scale bar, 50 μm. **(H)** Double immunofluorescence staining of F4/80 and iNOS in liver tissues. Nuclei were stained with DAPI. Scale bar, 50 μm. $*P < 0.05$, $**P < 0.01$.

prediction still need further analysis. In this study, we used WGCAN and LASSO-SVM analysis to identify 5 AH biomarkers co-associated with M1 macrophages, ferroptosis and cuproptosis in AH patients.

ALDOA is a key metabolic enzyme in glycolysis pathway. High expression of ALDOA is associated with poor prognosis in hepatocellular carcinoma (44). COL3A1 is a fibrous collagen found in connective tissue. Previous studies have shown that COL3A1 is involved in the progression of liver fibrosis (45). The levels of type III collagen formation and degradation were significantly increased in ALD patients compared to healthy

individuals (46). In addition, LUM has been identified as a biomarker for advanced fibrosis in non-alcoholic fatty liver disease (47). THBS2 is a novel biomarker for predicting the prognosis of metastatic pancreatic ductal adenocarcinoma (48). Manzardo et al. analyzed miRNA expression in alcoholics to further characterize the genetic influence of alcoholism and the influence of alcohol consumption on predicted target mRNA expression, which involved THBS2 (49). In mice treated with ethanol and CCl₄, down-regulation of TIMP1 effectively inhibited hepatic fibrosis and activation of hepatic stellate cell (50). Clinical studies have found that alcohol consumption in adolescents leads to
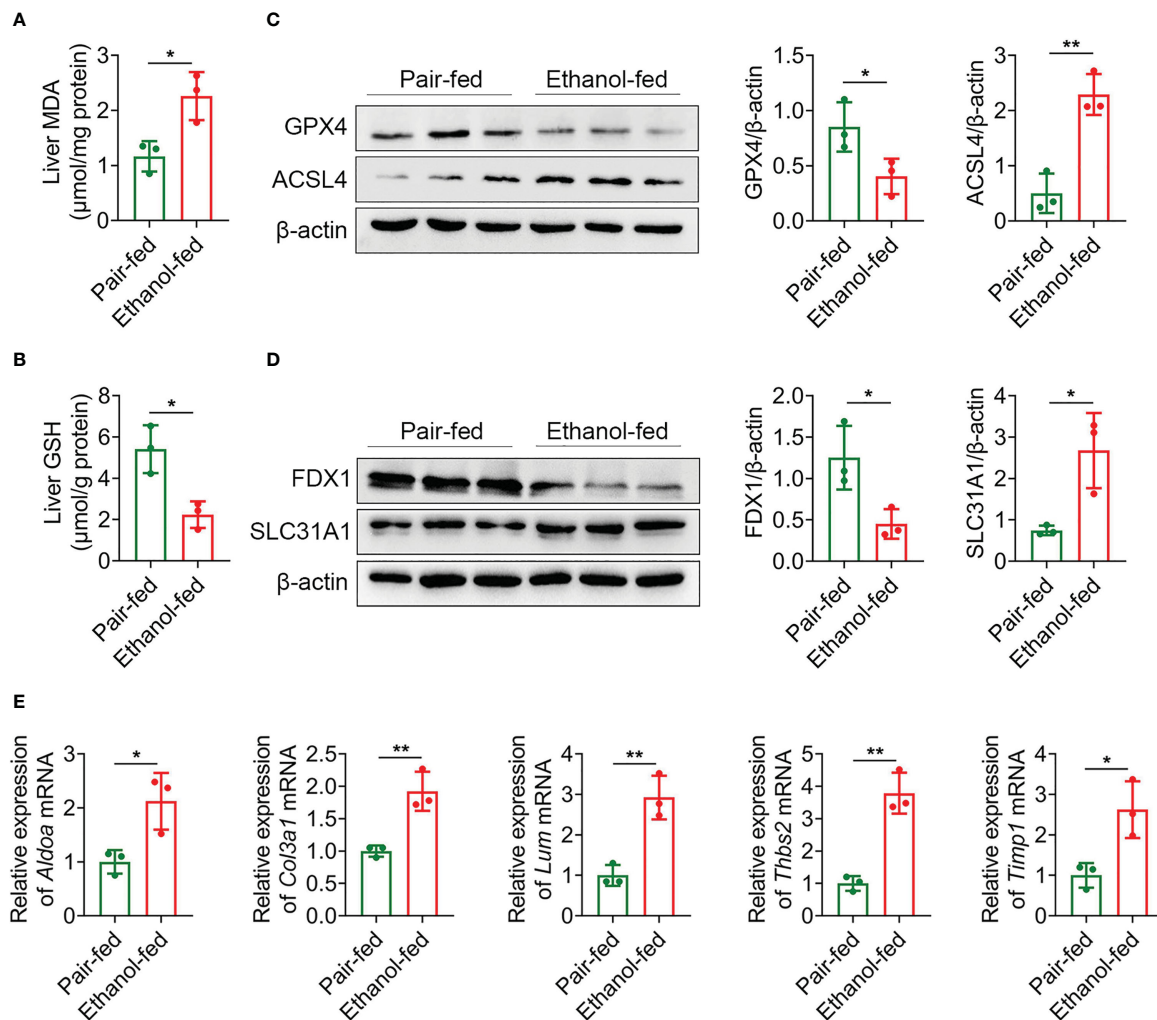
FIGURE 9

Alcohol exposure promotes the expression of ferroptosis, cuproptosis and potential biomarkers. **(A–E)** Groups of C57BL/6 mice (n = 5 per group) were fed ethanol liquid diet or ethanol free control liquid diet. **(A)** Content of MDA in liver tissues. **(B)** Content of GSH in liver tissues. **(C)** The protein expression levels of GPX4 and ACSL4 in liver tissues were determined using western blot analysis. The densities of protein were quantified using densitometry. GPX4 and ACSL4 were normalized to β-actin. **(D)** The protein expression levels of FDX1 and SLC31A1 in liver tissues were determined using western blot analysis. The densities of protein were quantified using densitometry. FDX1 and SLC31A1 were normalized to β-actin. **(E)** The mRNA levels of *Aldoa, Col3a1, Lum, Thbs2* and *Timp1* in liver tissues were measured using RT-qPCR analysis. The results were normalized to *Actb*. *P < 0.05, **P < 0.01.

elevated serum TIMP1 concentrations (51). We first reported that ALDOA, COL3A1, LUM, THBS2 and TIMP1 were highly expressed in AH and associated with M1 macrophages, ferroptosis and cuproptosis. Further studies with larger clinical cohorts and basic studies are needed to confirm these biomarkers.

Conclusion

In summary, we used CIBERSORT algorithm to analyze 22 types of immune cells, and M1 macrophages were the most significantly increased immune cells in AH patients. By combining bioinformatics analysis with a mouse model of AH, we identified 5 potential biomarkers co-associated with M1 macrophages, ferroptosis and cuproptosis. Further study of these

biomarkers can provide new ideas and basis for understanding the disease progression and targeted therapy of AH patients.

Data availability statement

The original contributions presented in the study are included in the article/Supplementary Material. Further inquiries can be directed to the corresponding author.

Ethics statement

The animal study was reviewed and approved by The Experimental Animal Ethics Committee of Mudanjiang Medical University.

Author contributions

Conception and design: QY. Data collection and analysis: SH, DW and QY. Manuscript writing: SH and XXY. Manuscript revising: XHY. All authors contributed to the article and approved the submitted version.

Funding

Acknowledgments

Conflict of interest

The authors declare that the research was conducted in the absence of any commercial or financial relationships that could be construed as a potential conflict of interest.

Publisher's note

All claims expressed in this article are solely those of the authors and do not necessarily represent those of their affiliated organizations, or those of the publisher, the editors and the reviewers. Any product that may be evaluated in this article, or claim that may be made by its manufacturer, is not guaranteed or endorsed by the publisher.

Supplementary material

The Supplementary Material for this article can be found online at: https://www.frontiersin.org/articles/10.3389/fimmu.2023.1146693/full#supplementary-material

References

1. Singal AK, Mathurin P. Diagnosis and treatment of alcohol-associated liver disease: A review. *JAMA* (2021) 326(2):165–76. doi: 10.1001/jama.2021.7683

2. Ventura-Cots M, Argemi J, Jones P, Lackner C, El Hag M, Abraldes J, et al. Clinical, histological and molecular profiling of different stages of alcohol-related liver disease. *Gut* (2022) 71(9):1856–66. doi: 10.1136/gutjnl-2021-324295

3. Sehrawat TS, Liu M, Shah VH. The knowns and unknowns of treatment for alcoholic hepatitis. *Lancet Gastroenterol Hepatol* (2020) 5(5):494–506. doi: 10.1016/S2468-1253(19)30326-7

4. Rattan P, Shah VH. Review article: current and emerging therapies for acute alcohol-associated hepatitis. *Aliment Pharmacol Ther* (2022) 56(1):28–40. doi: 10.1111/apt.16969

5. Arab JP, Diaz LA, Baeza N, Idalsoaga F, Fuentes-Lopez E, Arnold J, et al. Identification of optimal therapeutic window for steroid use in severe alcohol-associated hepatitis: A worldwide study. *J Hepatol* (2021) 75(5):1026–33. doi: 10.1016/j.jhep.2021.06.019

6. Furuya S, Argemi J, Uehara T, Katou Y, Fouts DE, Schnabl B, et al. A novel mouse model of acute-on-Chronic cholestatic alcoholic liver disease: A systems biology comparison with human alcoholic hepatitis. *Alcohol Clin Exp Res* (2020) 44(1):87–101. doi: 10.1111/acer.14234

7. Massey V, Parrish A, Argemi J, Moreno M, Mello A, Garcia-Rocha M, et al. Integrated multiomics reveals glucose use reprogramming and identifies a novel hexokinase in alcoholic hepatitis. *Gastroenterology* (2021) 160(5):1725–1740 e1722. doi: 10.1053/j.gastro.2020.12.008

8. Cho YE, Yu LR, Abdelmegeed MA, Yoo SH, Song BJ. Apoptosis of enterocytes and nitration of junctional complex proteins promote alcohol-induced gut leakiness and liver injury. *J Hepatol* (2018) 69(1):142–53. doi: 10.1016/j.jhep.2018.02.005

9. Wang C, Ma C, Gong L, Guo Y, Fu K, Zhang Y, et al. Macrophage polarization and its role in liver disease. *Front Immunol* (2021) 12:803037. doi: 10.3389/fimmu.2021.803037

10. Nowak AJ, Relja B. The impact of acute or chronic alcohol intake on the NF-kappaB signaling pathway in alcohol-related liver disease. *Int J Mol Sci* (2020) 21(24):9407. doi: 10.3390/ijms21249407

11. Zhao N, Xia G, Cai J, Li Z, Lv XW. Adenosine receptor A2B mediates alcoholic hepatitis by regulating cAMP levels and the NF-KB pathway. *Toxicol Lett* (2022) 359:84–95. doi: 10.1016/j.toxlet.2022.01.012

12. Cho Y, Joshi R, Lowe P, Copeland C, Ribeiro M, Morel C, et al. Granulocyte colony-stimulating factor attenuates liver damage by M2 macrophage polarization and hepatocyte proliferation in alcoholic hepatitis in mice. *Hepatol Commun* (2022) 6(9):2322–39. doi: 10.1002/hep4.1925

13. Santana-Codina N, Mancias JD. The role of NCOA4-mediated ferritinophagy in health and disease. *Pharm (Basel)* (2018) 11(4):114. doi: 10.3390/ph11040114

14. Tsvetkov P, Coy S, Petrova B, Dreishpoon M, Verma A, Abdusamad M, et al. Copper induces cell death by targeting lipoylated TCA cycle proteins. *Science* (2022) 375(6586):1254–61. doi: 10.1126/science.abf0529

15. Zhou Z, Ye TJ, DeCaro E, Buehler B, Stahl Z, Bonavita G, et al. Intestinal SIRT1 deficiency protects mice from ethanol-induced liver injury by mitigating ferroptosis. *Am J Pathol* (2020) 190(1):82–92. doi: 10.1016/j.ajpath.2019.09.012

16. Zhao Y, Zhang R, Wang Z, Chen Z, Wang G, Guan S, et al. Melatonin prevents against ethanol-induced liver injury by mitigating ferroptosis *via* targeting brain and muscle ARNT-like 1 in mice liver and HepG2 cells. *J Agric Food Chem* (2022) 70(40):12953–67. doi: 10.1021/acs.jafc.2c04337

17. Zhang Z, Zeng X, Wu Y, Liu Y, Zhang X, Song Z. Cuproptosis-related risk score predicts prognosis and characterizes the tumor microenvironment in hepatocellular carcinoma. *Front Immunol* (2022) 13:925618. doi: 10.3389/fimmu.2022.925618

18. Wang G, Xiao R, Zhao S, Sun L, Guo J, Li W, et al. Cuproptosis regulator-mediated patterns associated with immune infiltration features and construction of cuproptosis-related signatures to guide immunotherapy. *Front Immunol* (2022) 13:945516. doi: 10.3389/fimmu.2022.945516

19. Affo S, Dominguez M, Lozano JJ, Sancho-Bru P, Rodrigo-Torres D, Morales-Ibanez O, et al. Transcriptome analysis identifies TNF superfamily receptors as potential therapeutic targets in alcoholic hepatitis. *Gut* (2013) 62(3):452–60. doi: 10.1136/gutjnl-2011-301146

20. Trepo E, Goossens N, Fujiwara N, Song WM, Colaprico A, Marot A, et al. Combination of gene expression signature and model for end-stage liver disease score predicts survival of patients with severe alcoholic hepatitis. *Gastroenterology* (2018) 154(4):965–75. doi: 10.1053/j.gastro.2017.10.048

21. Liu M, Cao S, He L, Gao J, Arab JP, Cui H, et al. Super enhancer regulation of cytokine-induced chemokine production in alcoholic hepatitis. *Nat Commun* (2021) 12(1):4560. doi: 10.1038/s41467-021-24843-w

22. Khanova E, Wu R, Wang W, Yan R, Chen Y, French SW, et al. Pyroptosis by caspase11/4-gasdermin-D pathway in alcoholic hepatitis in mice and patients. *Hepatology* (2018) 67(5):1737–53. doi: 10.1002/hep.29645

23. Johnson WE, Li C, Rabinovic A. Adjusting batch effects in microarray expression data using empirical bayes methods. *Biostatistics* (2007) 8(1):118–27. doi: 10.1093/biostatistics/kxj037

24. Newman AM, Liu CL, Green MR, Gentles AJ, Feng W, Xu Y, et al. Robust enumeration of cell subsets from tissue expression profiles. *Nat Methods* (2015) 12(5):453–7. doi: 10.1038/nmeth.3337

25. Hänzelmann S, Castelo R, Guinney J. GSVA: gene set variation analysis for microarray and RNA-seq data. *BMC Bioinf* (2013) 17:7. doi: 10.1186/1471-2105-14-7

26. Fu J, Wang S, Li Z, Qin W, Tong Q, Liu C, et al. Comprehensive multiomics analysis of cuproptosis-related gene characteristics in hepatocellular carcinoma. *Front Genet* (2022) 13:942387. doi: 10.3389/fgene.2022.942387

27. Langfelder P, Horvath S. WGCNA: an r package for weighted correlation network analysis. *BMC Bioinf* (2008) 9:559. doi: 10.1186/1471-2105-9-559

28. Yu G, Wang LG, Han Y, He QY. clusterProfiler: an r package for comparing biological themes among gene clusters. *OMICS* (2012) 16(5):284–7. doi: 10.1089/omi.2011.0118

29. Walter W, Sanchez-Cabo F, Ricote M. GOplot: an r package for visually combining expression data with functional analysis. *Bioinformatics* (2015) 31 (17):2912–4. doi: 10.1093/bioinformatics/btv300

30. Ritchie ME, Phipson B, Wu D, Hu Y, Law CW, Shi W, et al. Limma powers differential expression analyses for RNA-sequencing and microarray studies. *Nucleic Acids Res* (2015) 43(7):e47. doi: 10.1093/nar/gkv007

31. Friedman J, Hastie T, Tibshirani R. Regularization paths for generalized linear models *via* coordinate descent. *J Stat Softw* (2010) 33(1):1–22. doi: 10.18637/jss.v033.i01

32. Karatzoglou A, Smola A, Hornik K, Zeileis A. Kernlab - an S4 package for kernel methods in r. *J Stat Software* (2004) 11(9):1–20. doi: 10.18637/jss.v011.i09

33. Robin X, Turck N, Hainard A, Tiberti N, Lisacek F, Sanchez J-C, et al. Proc: An open-source package for r and s+ to analyze and compare roc curves. *BMC Bioinf* (2011) 12:77. doi: 10.1186/1471-2105-12-77

34. Yuan Q, Hou S, Zhai J, Tian T, Wu Y, Wu Z, et al. S100A4 promotes inflammation but suppresses lipid accumulation *via* the STAT3 pathway in chronic ethanol-induced fatty liver. *J Mol Med (Berl)* (2019) 97(10):1399–412. doi: 10.1007/s00109-019-01808-7

35. Yuan Q, Zhang J, Liu Y, Chen H, Liu H, Wang J, et al. MyD88 in myofibroblasts regulates aerobic glycolysis-driven hepatocarcinogenesis *via* ERK-dependent PKM2 nuclear relocalization and activation. *J Pathol* (2022) 256(4):414–26. doi: 10.1002/path.5856

36. Szabo G, Petrasek J. Gut-liver axis and sterile signals in the development of alcoholic liver disease. *Alcohol Alcohol* (2017) 52(4):414–24. doi: 10.1093/alcalc/agx025

37. Hosseini N, Shor J, Szabo G. Alcoholic hepatitis: A review. *Alcohol Alcohol* (2019) 54(4):408–16. doi: 10.1093/alcalc/agz036

38. Enomoto N, Ikejima K, Bradford B, Rivera C, Kono H, Goto M, et al. Role of kupffer cells and gut-derived endotoxins in alcoholic liver injury. *J Gastroenterol Hepatol* (2000) Suppl:D20–25. doi: 10.1046/j.1440-1746.2000.02179.x

39. Ju C, Mandrekar P. Macrophages and alcohol-related liver inflammation. *Alcohol Res* (2015) 37(2):251–62.

40. Forrest E. Use of MELD scores in alcoholic hepatitis. *Lancet Gastroenterol Hepatol* (2020) 5(8):720. doi: 10.1016/S2468-1253(20)30194-1

41. Wang T, Dai L, Shen S, Yang Y, Yang M, Yang X, et al. Comprehensive molecular analyses of a macrophage-related gene signature with regard to prognosis, immune features, and biomarkers for immunotherapy in hepatocellular carcinoma based on WGCNA and the LASSO algorithm. *Front Immunol* (2022) 13:843408. doi: 10.3389/fimmu.2022.843408

42. Liu Z, Wang J, Li S, Li L, Li L, Li D, et al. Prognostic prediction and immune infiltration analysis based on ferroptosis and EMT state in hepatocellular carcinoma. *Front Immunol* (2022) 13:1076045. doi: 10.3389/fimmu.2022.1076045

43. Liu X, Sun B, Yao Y, Lai L, Wang X, Xiong J, et al. Identification of copper metabolism and cuproptosis-related subtypes for predicting prognosis tumor microenvironment and drug candidates in hepatocellular carcinoma. *Front Immunol* (2022) 13:996308. doi: 10.3389/fimmu.2022.996308

44. Wang J, Zhang HM, Dai ZT, Huang Y, Liu H, Chen Z, et al. MKL-1-induced PINK1-AS overexpression contributes to the malignant progression of hepatocellular carcinoma *via* ALDOA-mediated glycolysis. *Sci Rep* (2022) 12(1):21283. doi: 10.1038/s41598-022-24023-w

45. Tao R, Fan XX, Yu HJ, Ai G, Zhang HY, Kong HY, et al. MicroRNA-29b-3p prevents schistosoma japonicum-induced liver fibrosis by targeting COL1A1 and COL3A1. *J Cell Biochem* (2018) 119(4):3199–209. doi: 10.1002/jcb.26475

46. Thiele M, Johansen S, Gudmann NS, Madsen B, Kjaergaard M, Nielsen MJ, et al. Progressive alcohol-related liver fibrosis is characterised by imbalanced collagen formation and degradation. *Aliment Pharmacol Ther* (2021) 54(8):1070–80. doi: 10.1111/apt.16567

47. Chang Y, He J, Xiang X, Li H. LUM is the hub gene of advanced fibrosis in nonalcoholic fatty liver disease. *Clin Res Hepatol Gastroenterol* (2021) 45 (1):101435. doi: 10.1016/j.clinre.2020.04.006

48. Gimotty PA, Till JE, Udgata S, Takenaka N, Yee SS, LaRiviere MJ, et al. THSB2 as a prognostic biomarker for patients diagnosed with metastatic pancreatic ductal adenocarcinoma. *Oncotarget* (2021) 12(22):2266–72. doi: 10.18632/oncotarget.28099

49. Manzardo AM, Gunewardena S, Butler MG. Over-expression of the miRNA cluster at chromosome 14q32 in the alcoholic brain correlates with suppression of predicted target mRNA required for oligodendrocyte proliferation. *Gene* (2013) 526 (2):356–63. doi: 10.1016/j.gene.2013.05.052

50. Fujimoto Y, Kaji K, Nishimura N, Enomoto M, Murata K, Takeda S, et al. Dual therapy with zinc acetate and rifaximin prevents from ethanol-induced liver fibrosis by maintaining intestinal barrier integrity. *World J Gastroenterol* (2021) 27(48):8323–42. doi: 10.3748/wjg.v27.i48.8323

51. Zdanowicz K, Kowalczuk-Kryston M, Olanski W, Werpachowska I, Mielech W, Lebensztejn DM. Increase in serum MMP-9 and TIMP-1 concentrations during alcohol intoxication in adolescents-a preliminary study. *Biomolecules* (2022) 12 (5):710. doi: 10.3390/biom12050710